

Fixed Frequency Sliding Mode Control of Renewable Energy Resources in DC Micro Grid

Abdul Rehman Yasin, Muhammad Ashraf, Aamer Iqbal Bhatti and Ali Arshad Uppal

ABSTRACT

The rising cost of fossil fuels, their high depleting rate and issues regarding environmental pollution have brought the attention of the researchers towards renewable energy technologies. Different renewable energy resources like wind turbines, fuel cells and solar cells are connected to DC micro grid through controllable power electronic converters. In presence of these diverse generation units, robust controllers are required to ensure good power quality and to regulate grid voltage. This paper presents a sliding mode control based methodology to address the above mentioned challenges. The proposed technique keeps the switching frequency constant so that electromagnetic compatibility (EMC) issues can be solved with conventional filter design. Parallel operation of converter in DC micro grid is considered. Chattering reduction and power quality improvement by harmonic cancellation is proposed. A scaled down hardware for unregulated 11.5 V to 17.5 V input and 24V output is designed and tested. The experimental results show good performance of the controller under different loads and uncertain input voltage conditions. Moreover, the results show the robustness of the closed loop system to sudden variations in load conditions. Furthermore, a significant improvement in power quality is achieved by harmonic cancellation of chattering in the output of the converters.

Key Words: *Renewable Energy Resource, DC Micro Grids, Sliding Mode Control, DC-DC Converters, Power Engineering and Energy.*

I. Introduction

Micro grids are renowned for their advantages like sustained energy generation and appropriate utilization of distributed energy resources (DER). These DERs like solar cells, wind turbines, bio-gas installations and fuel cells are not located at a single sight and are interconnected to micro grids via controllable power electronic converters [1, 2]. These converters are scalable and show good conversion efficiencies

and add flexibility in the control process. Micro grid can be operated in grid connected or islanded mode [3, 4]. Numerous control strategies are implemented and developed for integrating DERs with central grid system. [5, 6, 7]

The major advantage of DC micro-grids over conventional AC transmission system is the absence of losses due to skin effect and reactive power flow. Moreover, micro grids are reliable, economical, efficient and easily manageable [8, 9, 10]. However, as DERs are connected to the same micro grid, the power converters responsible for power flow from these DERs operate in parallel. This creates challenges like voltage control of the grid, stability of parallel connected converters and load sharing among DERs [11, 12, 13].

The voltage of the DC grid is conventionally controlled by DC-DC converters [14, 15]. Buck

Abdul Rehman Yasin, Muhammad Ashraf and Aamer Iqbal Bhatti are with Department of Electrical Engineering, Capital University of Science and Technology (CUST), Islamabad Expressway, Kahuta Road, Zone-V Islamabad 44000, Pakistan. Ali Arshad Uppal is with Department of Electrical Engineering, COMSATS Institute of Information Technology, Islamabad, Pakistan.

converter has been proposed in [16] to control DC voltage in micro grid. The output voltage of buck converters is always lower than the input voltage. However, for photo-voltaic (PV) cells based applications where energy is harvested from solar radiations, it is required to boost the input voltages to draw maximum power from the PV cells [1]. Transformer based converter can efficiently provide higher output to input voltage ratio. But requirements in renewable energy applications like size, weight and cost makes transformerless converters a more appropriate choice. Because of the capability of boost converter to supply output voltage more than the input voltage, it is more feasible to be used in renewable energy applications [17, 18, 19].

Basic structure for voltage regulation in DC micro grid is shown in Fig. 1. Using a boost converter to control the voltage of a micro grid is a challenging problem because of its bilinear nature [20]. Bilinear systems belong to the class of non-linear systems where the non-linearity arises because of the product of control input with the system states [21]. Moreover, the system is non-minimum in phase and its linearized model has a right handed zero. This causes the dynamics of inductor current to become unstable if feedback design is based on measuring only the output voltage [22, 23, 24].

The issue of non-minimum phase can be avoided if the voltage regulation in boost converter is redefined as a current regulation problem [20, 25]. However, under uncertain load conditions a current regulator cannot keep its output voltage constant [26]. This makes the system extremely sensitive to load fluctuations. Fortunately, the current dynamics of boost converter are faster as compared to that of output voltage, therefore the issue can be resolved using a dual loop control structure. The inner current loop controls the power electronic switch based upon the reference signal provided by the outer voltage control loop [27].

Voltage regulation of DC bus bar is conventionally achieved by using PI controllers. The controllers act by increasing or decreasing the pulse width of the switching signal of the power converter. PI controllers are based on the average model of the converter which is linearized at a specific operating point to get the transfer function. Because of this constraint, their performance is degraded under large disturbance and load changes [28]. Moreover, under varying load conditions the PI gains need rapid tuning. Auto tuning methods are proposed in [29, 30] for PI, PD and PID controllers. But the schemes are rather complex than conventional PI controllers.

Researchers have proposed non-linear techniques to get better results. In [31] researcher have proposed

fuzzy logic control. Feed forward control is presented in [32, 33, 34], while H_∞ control is proposed in [35]. Even though the existing techniques have shown better performance however, they are not completely parameter invariant and more robust technique is required to deal with time varying and unknown load condition of micro grids.

Sliding mode controllers (SMC) are good choice to achieve the objective, because they provide parametric invariance and robustness [36, 37] against unknown disturbances. Moreover, as the power electronic switch in the converter operates in either on or off state. This makes SMC a natural choice to control such systems. Since SMC is a nonlinear control technique, it eliminates the need to obtain a linearized model of the power converter.

A major drawback in SM based controller is the varying switching frequency of the power converter. SM controllers do not provide a fixed switching frequency which causes the power electronic switch, in the converter, to operate under time varying frequency. This degrades the power quality and makes it difficult to suppress the electromagnetic emissions (EME) resulting from high current switching [38]. These emissions are filtered out by designing passive filters, so that the emissions do no interfere with nearby electronic components. The filter design depends upon the switching frequency, while variations in it makes the filter design non-trivial. Details of electromagnetic interference (EMI) and its importance in power converters can be found in [39]. The researchers have proposed variable hysteresis band modulation to address the issue [40]. The hysteresis band of the modulator is varied in such a way that the resulting switching frequency remains fixed. This controller design has relatively high implementation cost and is not feasible for commercial applications.

Therefore, the researchers have proposed fixed frequency SMC based on equivalent control signal [41, 42, 43]. However, because of non-minimum phase nature of boost converter, the controller designed to directly control its output voltage is not guaranteed to be stable [44]. A solution based on dual loop control structure is proposed in [45] where authors have shown that fixed frequency SMC achieves better dynamic response in DC micro grids. However, the double integral type sliding surface used by the authors to achieve faster dynamic response results in a non-symmetrical chattering signal that degrades the power quality and makes it non-trivial to apply harmonic cancellation techniques.

In the light of above discussion, it may be concluded that sufficient work has been reported

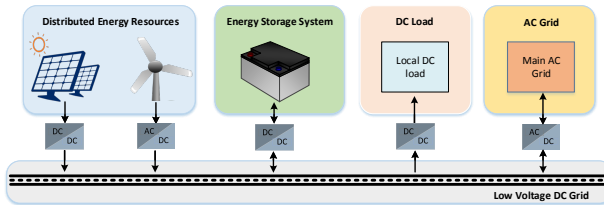


Fig. 1. Basic architecture of DC micro grid.

regarding voltage control in micro grids. However, according to the knowledge of the authors', discussion and solution to the issues regarding power quality in DC micro grids arising from the chattering problem are rare in the research community. Hence, there is a necessary need for addressing this issue along with achieving a robust, fixed frequency and parameter invariant solution.

In order to address the above mentioned challenges, this paper proposes a fixed frequency SMC along with harmonic cancellation of the chattering signal in a micro grid by utilizing an intuitive PI-type sliding manifold. A dual loop control structure is used, where the inner current loop is based on the proposed SMC technique with fixed switching frequency. The outer control loop is based upon a conventional PI controller which provides reference signal to the inner loop. The proposed methodology achieves a wide range stable operation along with addressing the load sharing problem of parallel connected converters in a micro grid. The objective of the paper is not only to achieve required robustness and harmonic cancellation of chattering but also to outline the hardware design approach in accordance with mathematical calculations, while ensuring the stability of the system. Hardware design based on low cost commercially available IC's is presented in order to avoid use of discrete time signal processors which are more sensitive to electromagnetic interference.

The rest of the article follows as: Mathematical model is presented in Section 2. Controller design is discussed in Section 3. Hardware setup is presented in Section 4, while experimental setup and results are presented in Section 5 and the article is concluded in Section 6.

II. Mathematical Model

The renewable energy resources and DERs supply power to the DC micro grid via controllable DC-DC converters as shown in Fig. 2. Their connection to the grid results in parallel operation of these converters as

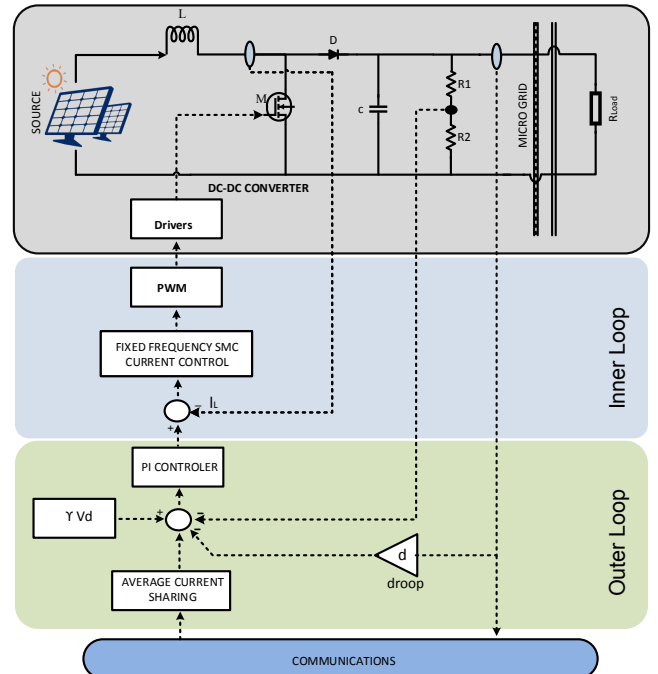


Fig. 2. Structure of control loops in DC micro grid using boost converter.

shown in Fig. 3. The input voltage from DER is denoted by V_{in} , whereas the output of the boost converter is V_{out} . The inductor current at any time is represented by I_L while C , L and R_L are the filter capacitance, inductance of coil and load resistance respectively. By the application of fundamental laws of circuit analysis, following mathematical model is obtained:

$$\frac{d}{dt} I_L = \frac{1}{L} V_{out}(u - 1) + \frac{V_{in}}{L} \quad (1)$$

$$\frac{d}{dt} V_{out} = \frac{1}{C} I_L(1 - u) - \frac{V_{out}}{R_L C} \quad (2)$$

For the sake of simplicity of mathematical analysis, we substitute $\tilde{u} = (1 - u)$. Since the power electronic converters are designed to operate only in ON and OFF states, thus the control signal can only take value from a discrete set of $\{1, 0\}$. The value of the switch with respect to its conduction state is defined as:

$$f(x) = \begin{cases} 1, & \text{Switch is conducting} \\ 0, & \text{Switch is open circuited} \end{cases} \quad (3)$$

The equilibrium points of the converter are found by setting all the time derivatives equal to zero in (2), and we get:

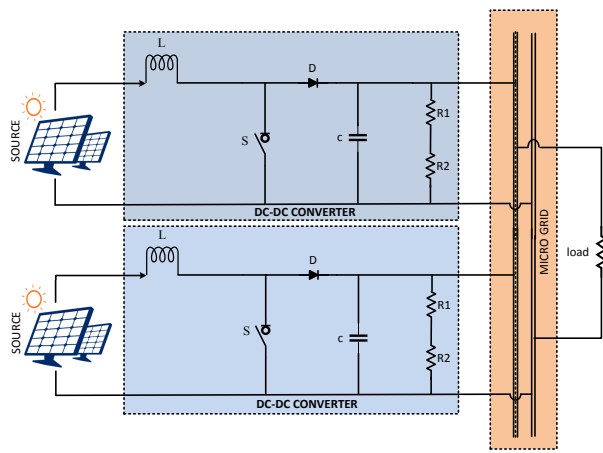


Fig. 3. Block diagram showing parallel operation of power converter in a DC micro grid.

$$V_{out} = V_d \quad (4)$$

$$I_{L_{eq}} = \frac{V_d^2}{R_L V_{in}} \quad (5)$$

where V_d is the desired output voltage and $I_{L_{eq}}$ is the inductor current at equilibrium point.

III. Controller Design

SMC is a non-linear control technique where the control signal is switched between two values to enforce the state trajectories to slide along a plane (sliding surface) in the state space. This control mechanism can be divided into two phases. In the first phase, also known as the reaching phase, the control law enforces the trajectories to reach the sliding surface σ irrespective of their initial values. Satisfying the hitting condition [46] is sufficient to ensure that the states will reach the sliding surface from irrespective of their initial values, hence we use the control law as [20]:

$$u = \frac{1}{2}(1 + sign(\sigma)) \quad (6)$$

When the state trajectories have reached the sliding surface, the second phase of SM control starts. In this phase the control law forces the trajectories to slide along the sliding surface towards the origin. The sliding surface is designed in such a way that when the trajectories reach the origin, the output voltage of

converter equals the desired grid voltage. To achieve the objective a PI-type sliding surface is designed as:

$$\sigma = k_1 \int e_i(t) dt + k_2 e_i(t) \quad (7)$$

where k_1, k_2 are positive design constants and $e_i(t)$ is the current error defined as:

$$e_i(t) = I_{ref} - I_L \quad (8)$$

where I_{ref} is the reference inductor current provided by the outer PI voltage control loop. The derivation of constant frequency SMC is based on equivalent control [46] method. The equivalent control signal u_{eq} is a theoretical continuous time signal that replaces the discontinuous control signal for the sake of mathematical analysis. The expression of u_{eq} for this system under sliding mode is computed by equating the time derivative of the sliding surface to zero. Thus we get:

$$\dot{\sigma} = k_1 e_i(t) + k_2 \dot{e}_i(t) = 0 \quad (9)$$

By using (2) and (9) we get:

$$\tilde{u}_{eq} = \frac{V_{in}}{V_{out}} - \frac{k_1}{k_2} \frac{L}{V_{out}} e_i(t) \quad (10)$$

We derive the equivalent control for the system by substituting $\tilde{u}_{eq} = (1 - \tilde{u}_{eq})$ and using (8) we get:

$$u_{eq} = (1 - \frac{V_{in}}{V_{out}}) + \frac{k_1}{k_2} \frac{L}{V_{out}} (I_{ref} - I_L) \quad (11)$$

After the establishment of SM control when $\sigma = 0$ is achieved, the equivalent control of the system equals the duty ration d in PWM converters [47].

$$u_{eq} = d = \frac{V_c}{V_{Pr}} \quad (12)$$

$$V_c = u_{eq} \times V_{Pr} \quad (13)$$

where V_{Pr} is the peak amplitude of ramp signal and V_c is the SM control based control signal which is PWM modulated to get a discontinuous control for the power electronic switch having a fixed switching frequency [47]. By using (11) and (13) and selecting ($V_{Pr} = V_{out}$) we get the control equation as:

$$V_c = (V_{out} - V_{in}) + L \frac{k_1}{k_2} (I_{ref} - I_L) \quad (14)$$

and the peak of ramp signal V_{Pr} as:

$$V_{Pr} = V_{out} \quad (15)$$

The equivalent control is a theoretical signal that completely describes the sliding motion when $\dot{\sigma} = \sigma = 0$ has been established [46]. Taking Laplace transform of $\dot{\sigma} = 0$ in (9) we get:

$$Sk_2 E_i(S) + k_1 E_i(S) = 0 \quad (16)$$

The time domain solution of (16) ensures that $e_i(t) \rightarrow 0$ and $V_{out} \rightarrow V_d$. Substituting these values in (14) and (15) we get:

$$V_c = (V_d - V_{in}) + L \frac{k_1}{k_2} (I_{ref} - I_L) \quad (17)$$

and the peak of ramp signal V_{Pr} as:

$$V_{Pr} = V_d \quad (18)$$

It shall be noticed that the proposed control structure in (17) does not have any adaptive tuning of V_{Pr} , as in previously proposed work in fixed frequency SMC. This simplifies the hardware implementation and solves the problem of modulation non-linearities which arise due to changing amplitude of modulating ramp signal. The structure of (17) contains the term $(V_d - V_{in})$ which acts as feed forward gain and helps achieve smaller settling time as compared to conventional PID controllers.

3.1. Stability of the Controller

Sliding mode can exist on the manifold $\sigma = 0$ if the following condition is satisfied [20].

$$\lim_{\sigma \rightarrow 0} \sigma \dot{\sigma} < 0 \quad (19)$$

By using (2) and (7) we derive the expression for $\dot{\sigma}$ as:

$$\dot{\sigma} = k_1 e_i(t) + \tilde{u} \frac{k_2}{L} V_{out} - \frac{k_2}{L} V_{in} \quad (20)$$

when $\sigma \rightarrow 0^+$ then according to (19), $\dot{\sigma} < 0$ thus (20) is written as:

$$k_1 e_i(t) + \tilde{u} \frac{k_2}{L} V_{out} - \frac{k_2}{L} V_{in} < 0 \quad (21)$$

As $\sigma \rightarrow 0^+$, the control law (6) turns $u = 1$ ($\tilde{u} = 0$) and thus (21) is written as:

$$k_1 e_i(t) - \frac{k_2}{L} V_{in} < 0 \quad (22)$$

Since V_{in} is always positive, thus (22) is ensured to hold true if the following condition is fulfilled.

$$\frac{k_2}{L} V_{in} > k_1 \|e_i(t)\| \quad (23)$$

When $\sigma \rightarrow 0^-$ then according to (19), $\sigma > 0$ and we write (20) as:

$$k_1 e_i(t) + \tilde{u} \frac{k_2}{L} V_{out} - \frac{k_2}{L} V_{in} > 0 \quad (24)$$

As $\sigma \rightarrow 0^-$ the control law (6) turns $u = 0$ ($\tilde{u} = 1$) and (24) is written as:

$$k_1 e_i(t) + \frac{k_2}{L} V_{out} - \frac{k_2}{L} V_{in} > 0 \quad (25)$$

The following conditions shall be satisfied to ensure that (25) remains true.

$$\frac{k_2}{L} \|(V_{out} - V_{in})\| > k_1 \|e_i(t)\| \quad (26)$$

For boost converter $V_{out} > V_{in}$ and hence (23) and (26) are easily satisfied by appropriate selection of k_1 and k_2 .

3.2. Parameterization of Controller

In this subsection calculations for the specific case are presented while design procedure for general case is given in the Appendix A. Both V_{in} and V_{out} exceed the maximum allowable limits of op-amps and are fed through a resistor network with attenuation constant β . By selecting reference voltage V_{ref} of 2.5 V we calculate β as:

$$\beta = \frac{V_{ref}}{V_d} = \frac{2.5}{24} = 0.104 \quad (27)$$

Selecting $R_1 = 6.8 \text{ k}\Omega$, R_2 is computed as:

$$R_2 = \frac{\beta}{1 - \beta} R_1 = 789 \Omega \quad (28)$$

The constant β is multiplied and divided in the control law as:

$$u_{eq} = \frac{\beta V_c}{\beta V_{Pr}} = \frac{V_c^*}{V_{Pr}^*} \quad (29)$$

where

$$V_c^* = \beta V_d - \beta V_{in} - \beta L \frac{k_1}{k_2} (I_{ref} - I_L) \quad (30)$$

and peak of ramp signal becomes:

$$V_{Pr}^* = \beta V_d \quad (31)$$

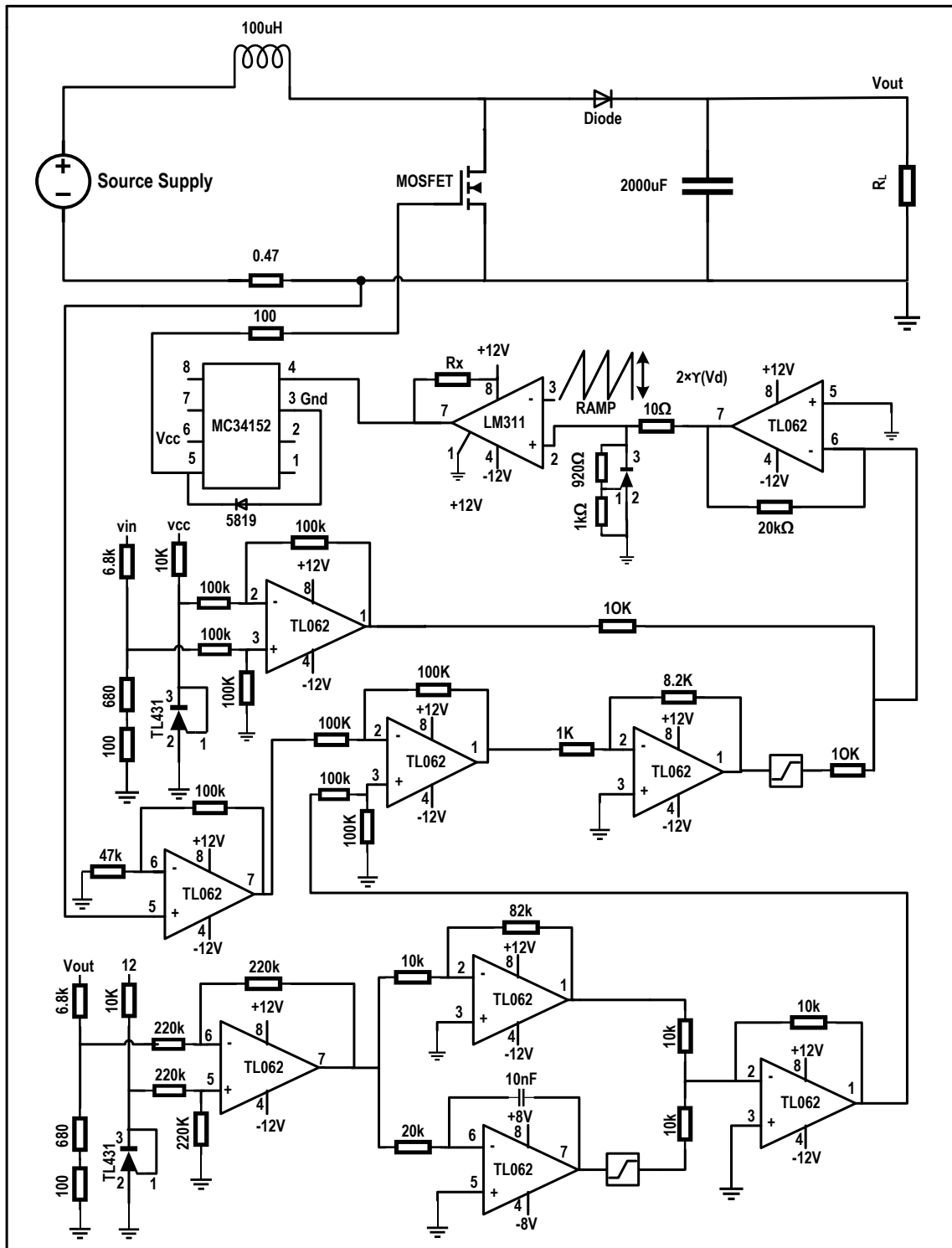


Fig. 4. Schematic of the proposed technique for voltage regulation in a single renewable energy resource.

To use TL431 and limit the maximum duty cycle, gain of two is applied to both V_{Pr} and V_c^* . This gain has no effect on control law as same constant is multiplied in numerator and denominator of equation (12). The constraints for the stability in (23) and (26) becomes:

$$\beta \frac{k_2}{L} V_{in} > k_1 \|e_i(t)\| \quad (32)$$

$$\beta \frac{k_2}{L} \|(V_{out} - V_{in})\| > k_1 \|e_i(t)\| \quad (33)$$

It is important to mention that the output of the operational amplifiers computing $k_1 e_i(t)$ is limited to ± 5 V, thus mathematically $k_1 \|e_i(t)\| \leq 5$. By proper selection of k_2 the constraints (32) and (33) are easily satisfied.

3.3. Selection of Sliding Constants

When the system has entered the sliding phase then the dynamics of the system are completely described by manifold $\sigma = 0$, thus by using (7) we get:

$$k_1 \int e_i(t) dt + k_2 e_i(t) = 0 \quad (34)$$

Taking time derivative of (34) we get:

$$k_1 e_i(t) + k_2 \dot{e}_i(t) = 0 \quad (35)$$

$$\dot{e}_i(t) = -\frac{k_1}{k_2} e_i(t) \quad (36)$$

Since k_1 and k_2 are positive design constants, hence as $t \rightarrow \infty$, $e_i(t) \rightarrow 0$. The rate of decay of $e_i(t)$ is controlled by the ratio of k_1 to k_2 . The time domain solution of (36) is:

$$e_i(t) = e_{io} e^{-(\frac{k_1}{k_2})t} \quad (37)$$

where e_{io} is the initial value of error. It is important to note that the decay rate of the error signal is controlled by the ratio of k_1 to k_2 . Large values of k_1/k_2 leads to faster decay of the error but at the cost of increased control effort (large duty ratio). This causes high inrush current at the start up of the converter which may trigger the over circuit protection circuits in the source supply (renewable energy resource). Hence there is a compromise in selection of the ratio. Primarily, the constants k_1 and k_2 are selected such that constraint for stability in (32) is satisfied. We select $(\beta k_2 V_{in}/L)$ to be 12 times greater than $k_1 e_i(t)$, hence the inequality (32) is transformed into equation as:

$$\beta \frac{k_2}{L} V_{in} = 12 k_1 \|e_i(t)\| \quad (38)$$

Table 1. Voltage regulation at different input source voltages.

Reading No.	Input source voltage	Output Voltage
1	11.5	24.0
2	13.0	24.0
3	14.5	24.0
4	16.0	24.0
5	17.5	24.0

For $V_{in} = 12$ V, $L = 100 \times 10^{-6}$ H, we select $k_1/k_2 = 80 \times 10^4$. As discussed in Section 3.2 the maximum value of $\|k_1 e_i(t)\|$ is 5, hence using equation (38) we get $k_2 = 4.8 \times 10^{-3}$ and $k_1 = 3.84 \times 10^3$. The values satisfy both the constraints in (32) and (33).

IV. Hardware Description

The boost converter used in the experiments has filter capacitance, $C = 2000 \mu F$, and inductor coil having $L = 100 \mu H$. A metal oxide field effect transistor (MOSFET), IRF540 is used as power electronic switch. Its on resistance is 0.06Ω and can sustain a continuous drain current of 20 A. The selected switching frequency for fixed frequency SMC is 32 kHz. The selection of switching frequency is a compromise between switching losses and maximum allowable amplitude of chattering (ripples in the output). The efficiency of the converter also decreases with increasing switching frequency because of increase in switching losses. The designed converter has an efficiency of 92%. Experiments reveal that for proper switching of the MOSFET, the resistance seen at the drain of the device shall be less than 47Ω , so that the body diode capacitance of the device can be easily discharged. If this issue is not taken care off, then it may take significantly high time for the MOSFET to turn off. To ensure discharge of gate capacitance a resistor of $47 k\Omega$ is placed between gate and source of the device. Adjustable shunt type voltage regulator TL431 is used to generate reference signal of 2.5 V. The inductor current is measured by placing a resistor $R_{Me} = 0.47 \Omega$, in the return path of I_L . By Ohm's law $I_L = V_{Me}/R_{Me} = 2.1V_{Me}$. Thus the voltage V_{Me} is amplified by a gain of 2.1, before being fed to the controller circuitry.

V. Experimental Setup and Results

The experiments are performed using Rigol oscilloscope having two channels of 70 MHz bandwidth.

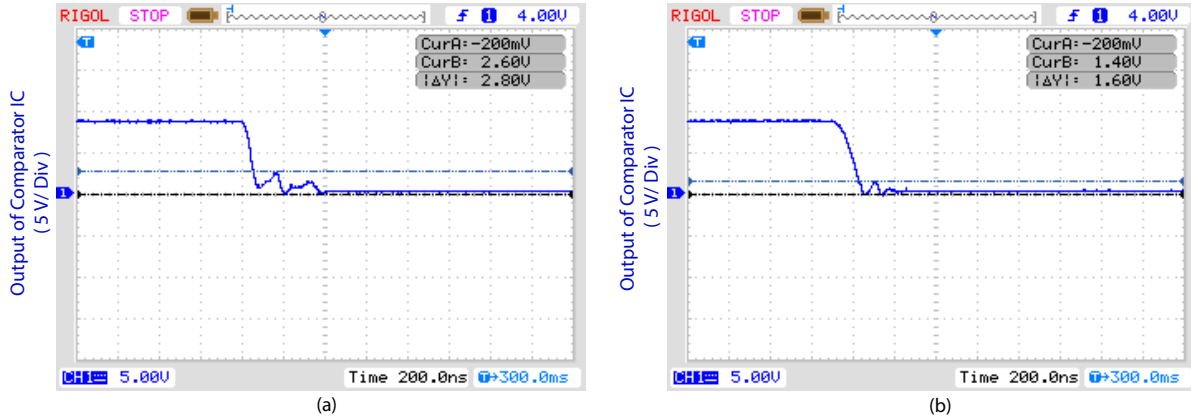


Fig. 6. Output of comparator IC LM311 showing oscillations at crossover (a) For $R_x = 1 \text{ k}\Omega$ and $V_{cc} = 9 \text{ V}$ (b) For $R_x = 333 \Omega$ and $V_{cc} = 9 \text{ V}$.

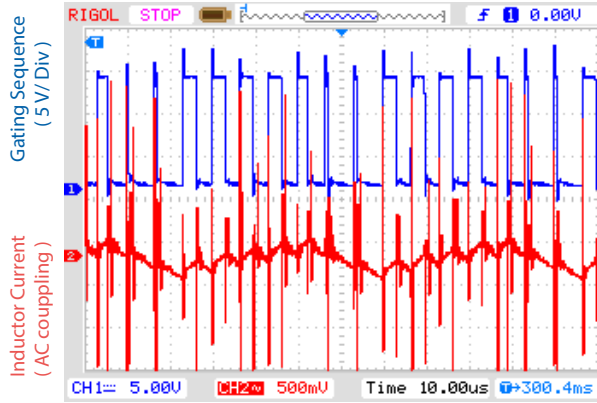


Fig. 5. The CH. 1 shows chattering along with low frequency oscillations for $R_x = 10 \text{ k}\Omega$ while CH. 2 shows the generated gating sequence as a consequence of improper selection of R_x .

The maximum sampling rate is 1G samples/sec. To record the controller behavior under varying input voltages, Matrix precision supplies accurate to 0.1 decimal place are used. The op-amps are powered with $\pm 15 \text{ V}$ using same power supplies. The steady state behavior is measured with oscilloscope settings of 10 V/div. It is worth mentioning that at 5 V/div and 10 V/div settings, the oscilloscope has an accuracy to one decimal place. Thus any voltage above 23.95 V will be rounded off to 24.0 V.

5.1. Pulse Width Modulation Circuit

PWM signal is generated using IC (LM311) that compares V_c with a ramp signal having peak amplitude of V_{Pr} . This comparator IC (LM311) has an advantage of isolated common mode input. The design engineer has a liberty to refer the output of the comparator to

ground or V_{cc} . Referring the output of the IC to ground inverts the output signal with respect to input signal. However, it is important to mention that the rise time of the output pulse depends upon the resistor R_x in Fig. 4. For large values of R_x , the rise time of the output pulse is significantly high and it takes large time to reach 1.75 V which is logic 1 for MOSFET gate driver MC34152. This causes a significant delay in the switching command to MOSFET. For example with $R_x = 10 \text{ k}\Omega$ and frequency of ramp signal $f_s = 150 \text{ kHz}$, the duty ratio can not exceed 42% even when $V_{out} = 0$ (feedback signal disconnected). This is a non-linear behavior which is introduced because of high rise time of the comparator when R_x is not properly selected. In this case the comparator IC fails to generate a duty ratio equal to (V_c/V_{Pr}) . As a result a false duty cycle is generated that increases I_L in each switching cycle, causing V_{out} to increase. The controller generates lower V_c to control the output voltage drift but because of above mentioned non-linearity, the duty cycle does not change accordingly. Finally the output increases to a level where the controller makes the duty ratio significantly small resulting in decreasing the inductor current in successive cycles. This results in low frequency oscillations in the output voltage other than chattering (ripples in power electronic literature). These low frequency oscillations along with the gating signal are shown in Fig. 5. It shall be noticed that this non-linearity is a type of actuator saturation and belongs to a class of unmatched disturbances and can not be canceled by SMC. Thus it is important to eliminate them in proper hardware design. For mid range values of R_x the output of comparator may oscillate at crossing points as shown in Fig. 6(a). This may occur when one of the inputs is a ramp signal or the source resistance generating input signal is high. The

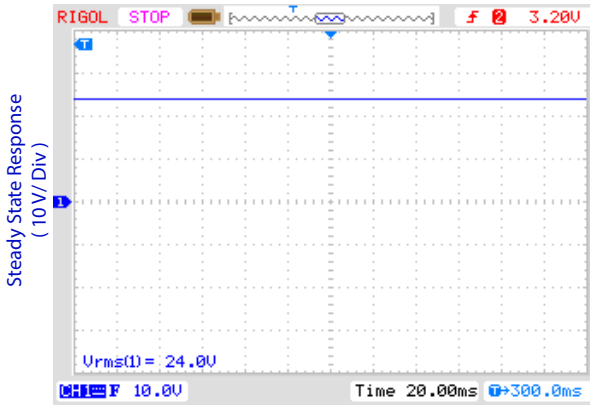


Fig. 7. Steady state response of the closed loop system.

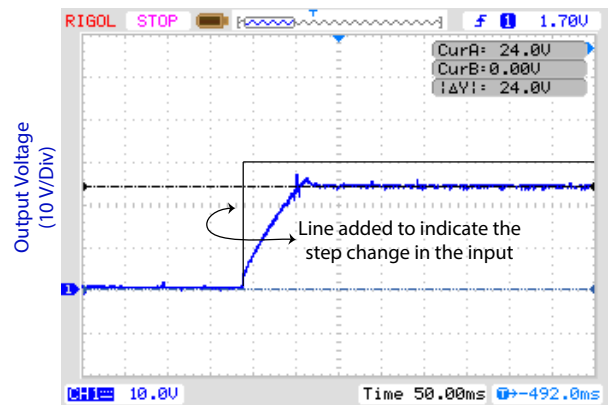
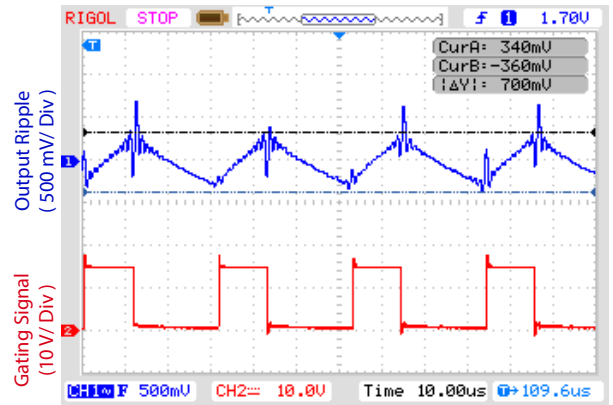
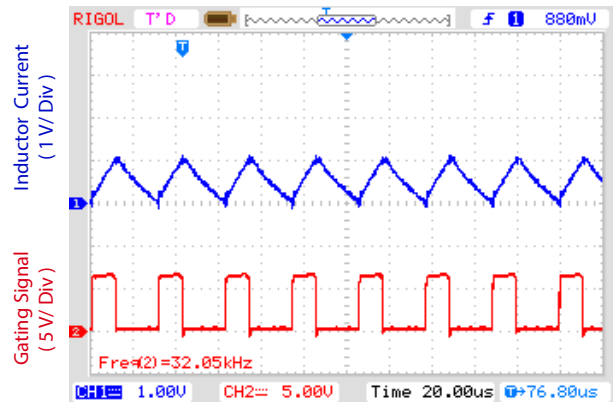
problem is solved by adding a small hysteresis band using positive feedback or by lowering both R_x and the supply voltage of LM311. Lowering R_X and the supply voltage of LM311 also lowers the peak of oscillations at crossover to be less than 1.75 V and hence MC34152 will not get false trigger as shown in Fig. 6(b).

5.2. Step Response of the Closed Loop System

The performance of the controller is tested at different load conditions. The input voltage of the converter is switched at 400 mHz to obtain step response of the system. The switching action is accomplished by TIP147, a PNP power transistor, that connects and disconnects V_{in} according to a 400 mHz square wave. The complete response of the closed loop system is shown in Fig. 8. The controller maintains 24 V for different load condition ($18 \Omega \leq R_L \leq 100 \Omega$) and the output is shown in Fig. 7. The steady state error of the controller is zero because of the presence of an integrator in the outer voltage control loop. The output ripple during steady state operation is shown in Fig. 9. The inductor current at steady state is shown in Fig. 10. It is obtained by blocking the DC contents of the signal and using ‘AC coupling’ option of the oscilloscope. Fig. 9 and Fig. 10 shows the gating signal at the output of comparator IC LM311 and MOSFET driver MC34152 respectively. The major advantage of MC34152 is its high slew rate that reduces switching losses.

5.3. Robustness to Load and Line Variations

To verify the robustness of the controller and note its behavior under changing load conditions, a setup is designed to switch load resistance from 82Ω to 29.87Ω . This is accomplished by switching a

Fig. 8. Complete response of the system with step change in input voltage from 0 V to V_{in} .Fig. 9. The CH. 1 shows the ripple/chattering in the output voltage at 82Ω load resistor while CH. 2 shows the gating signal at the output of MC34152.Fig. 10. The CH. 1 shows the inductor current at steady state when operating at 82Ω load resistor while CH. 2 shows the gating signal observed at the output of LM311.

$82\ \Omega$ resistor in parallel to the existing $47\ \Omega$ load. A power transistor TIP147 driven by C1383 is used to switch this additional load at a frequency of 10 kHz. Fig. 11 shows the output of the converter when the load is changed from $82\ \Omega$ to $29.87\ \Omega$. The system recovers from the step load change in less than 250 ns. This demonstrates excellent disturbance rejection performance of the controller which is the key feature of SMC. Moreover, the performance of the controller under variable input voltages is also tested and the observations are presented in Table 1.

5.4. Grid Operation

The ability of the technique to control a DC micro grid is evaluated on a scaled down micro grid having two sources and a single load as shown in Fig. 3. An outer control loop provides reference current signal for both the sources operated by the proposed controller. Fig. 12 shows the currents of each source while feeding a load of $56\ \Omega$. The current delivered by Source 1 is 208 mA, while Source 2 contributes current of 210 mA. The proposed technique maintains the desired grid voltage with load sharing error of less than 1%. Fig. 13 shows the complete hardware setup for the closed loop system. Due to the fixed switching frequency of the proposed technique, harmonic cancellation of chattering is possible. Chattering is reduced in the proposed technique by adjusting the phase of two switching sequences such that the harmonics present in chattering signal of Source 1 are canceled by the harmonic contents in chattering signal of Source 2. Fig. 14(a) shows the chattering due to single source having peak-peak amplitude of 180 mV with RMS value of 59.3 mV. A significant reduction in chattering is observed when the phase of the switching sequence of Source 2 is adjusted to cancel the harmonic contents of chattering due to Source 1. Fig 14(b) shows that the RMS value of chattering falls to 16 mV only, while its peak-peak amplitude is reduced to only 56 mV.

VI. Conclusion

In this research the voltage control of DC bus bar in micro grids under uncertain load conditions is addressed. The experimental results show that the proposed technique is robust against input voltage variations and load changes, while maintaining fixed switching frequency. The paper discusses the circuit design and component selection in detail. The results show the good performance of the closed loop system based on renewable energy resources. Furthermore, the

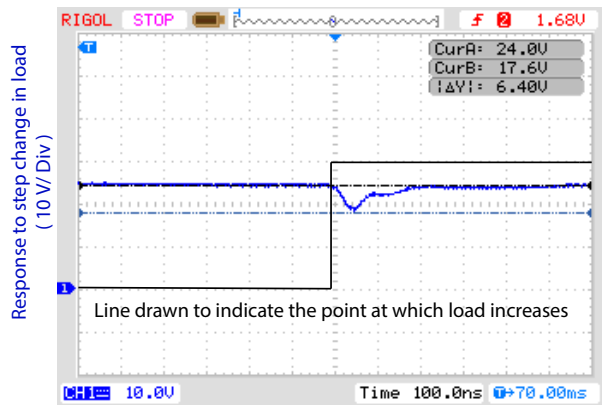


Fig. 11. Response of the system to step change in load from $82\ \Omega$ to $29.87\ \Omega$

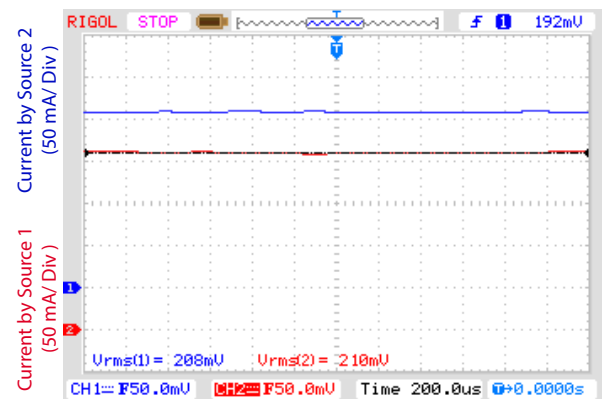


Fig. 12. Current sharing of the two sources using proposed controller.



Fig. 13. Hardware setup for the closed loop system.

technique is demonstrated on a scaled down micro grid with two sources. Improvement of power quality by harmonic cancellation of chattering is demonstrated in the hardware.

In modern renewable energy systems, the economics related to the produced energy is of great importance. Therefore, the future work it is intended to evaluate the proposed technique on the basis of fuel

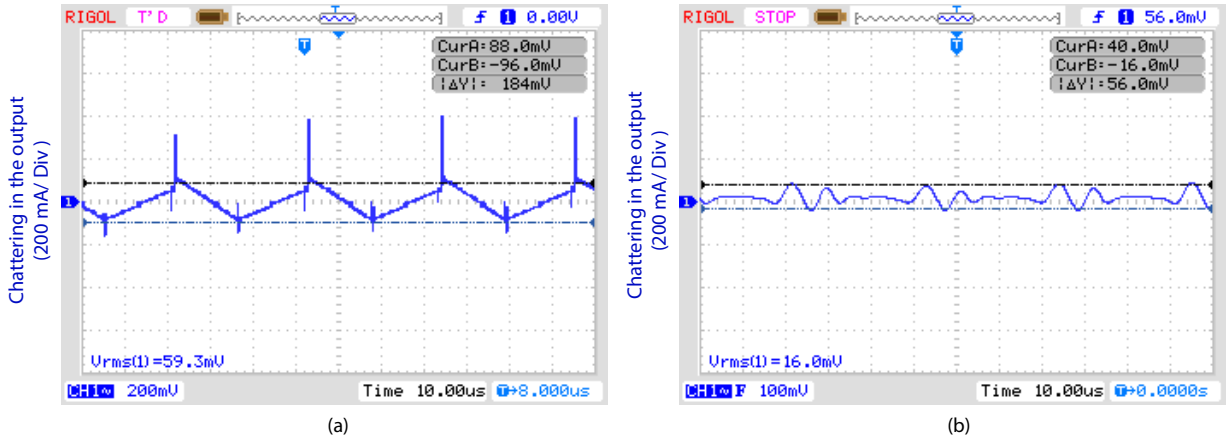


Fig. 14. Harmonic cancellation of chattering in the output (a) Chattering due to single source. (b) Chattering in the output when the harmonics in chattering signal of Source 2 cancels the harmonics from Source 1.

economy and efficiency of the closed loop system.

Appendix

A. Design Procedure of the Proposed Technique for General Case

Step 1: Choose an appropriate reference voltage V_{ref} and calculate attenuation constant β according to the desired output voltage V_d using following equation:

$$\beta = \frac{V_{ref}}{V_d}$$

Step 2: Select a standard value resistor for R_2 and calculate R_1 as:

$$R_1 = \frac{(1 - \beta)}{\beta} R_2$$

Step 3: Choose the ratio k_1/k_2 according to the following equation:

$$\beta \frac{k_2}{L} V_{in} = 12k_1 \|e_i(t)\|$$

Step 4: Check that the values of k_1 and k_2 calculated in Step 3 satisfy the following two constraints:

$$\beta \frac{k_2}{L} V_{in} > k_1 \|e_i(t)\|$$

$$\beta \frac{k_2}{L} \|(V_{out} - V_{in})\| > k_1 \|e_i(t)\|$$

Step 5: Compute the equation of V_c^* as:

$$V_c^* = \beta V_d - \beta V_{in} - \beta L \frac{k_1}{k_2} (I_{ref} - I_L)$$

Step 6: Set the peak amplitude of the ramp signal V_{Pr}^* as:

$$V_{Pr}^* = \beta V_d$$

REFERENCES

1. A. Yahya, H. El Fadil, M. Oulcaid, L. Ammeh, F. Giri, and J. M. Guerrero, "Control of grid connected photovoltaic systems with microinverters: New theoretical design and numerical evaluation," *Asian Journal of Control*, vol. 20, no. 2, pp. 906–918, 2018.
2. T. Morstyn, B. Hredzak, and V. G. Agelidis, "Control strategies for microgrids with distributed energy storage systems: An overview," *IEEE Transactions on Smart Grid*, vol. 9, no. 4, pp. 3652–3666, 2018.
3. M. Armin, P. N. Roy, S. K. Sarkar, and S. K. Das, "Lmi-based robust pid controller design for voltage control of islanded microgrid," *Asian Journal of Control*, vol. 20, no. 5, pp. 2014–2025, 2018.
4. G. G. Talapur, H. Suryawanshi, L. Xu, and A. Shitole, "A reliable micro-grid with seamless transition between grid connected and islanded mode for residential community with enhanced power quality," *IEEE Transactions on Industry Applications*, 2018.
5. K. E. Antoniadou-Plytaria, I. N. Kouveliotis-Lysikatos, P. S. Georgilakis, and N. D. Hatziargyriou, "Distributed and decentralized voltage control of smart distribution networks: models, methods, and future research," *IEEE Transactions on Smart Grid*, vol. 8, no. 6, pp. 2999–3008, 2017.

6. X. Wang, L. Harnefors, and F. Blaabjerg, “Unified impedance model of grid-connected voltage-source converters,” *IEEE Transactions on Power Electronics*, vol. 33, no. 2, pp. 1775–1787, 2018.
7. Y. Guan, L. Meng, C. Li, J. C. Vasquez, and J. M. Guerrero, “A dynamic consensus algorithm to adjust virtual impedance loops for discharge rate balancing of ac microgrid energy storage units,” *IEEE Transactions on Smart Grid*, vol. 9, no. 5, pp. 4847–4860, 2018.
8. H. Lotfi and A. Khodaei, “Ac versus dc microgrid planning,” *IEEE Transactions on Smart Grid*, vol. 8, no. 1, pp. 296–304, 2017.
9. L. Herrera, W. Zhang, and J. Wang, “Stability analysis and controller design of dc microgrids with constant power loads,” *IEEE Trans. Smart Grid*, vol. 8, no. 2, pp. 881–888, 2017.
10. C. Li, F. De Bosio, F. Chen, S. K. Chaudhary, J. C. Vasquez, and J. M. Guerrero, “Economic dispatch for operating cost minimization under real-time pricing in droop-controlled dc microgrid,” *IEEE Journal of Emerging and Selected Topics in Power Electronics*, vol. 5, no. 1, pp. 587–595, 2017.
11. A. Bonfiglio, M. Brignone, F. Delfino, and R. Procopio, “Optimal control and operation of grid-connected photovoltaic production units for voltage support in medium-voltage networks,” *IEEE Transactions on Sustainable Energy*, vol. 5, no. 1, pp. 254–263, 2014.
12. M. Su, Z. Liu, Y. Sun, H. Han, and X. Hou, “Stability analysis and stabilization methods of dc microgrid with multiple parallel-connected dc–dc converters loaded by cpls,” *IEEE Transactions on Smart Grid*, vol. 9, no. 1, pp. 132–142, 2018.
13. C. Wang, J. Duan, B. Fan, Q. Yang, and W. Liu, “Decentralized high-performance control of dc microgrids,” *IEEE Transactions on Smart Grid*, 2018.
14. Y. Li, L. He, F. Liu, C. Li, Y. Cao, and M. Shahidehpour, “Flexible voltage control strategy considering distributed energy storages for dc distribution network,” *IEEE Transactions on Smart Grid*, 2017.
15. S. Augustine, M. K. Mishra, and N. Lakshminarasamma, “Adaptive droop control strategy for load sharing and circulating current minimization in low-voltage standalone dc microgrid,” *IEEE Transactions on Sustainable Energy*, vol. 6, no. 1, pp. 132–141, 2015.
16. S. Anand, B. G. Fernandes, and J. Guerrero, “Distributed control to ensure proportional load sharing and improve voltage regulation in low-voltage dc microgrids,” *IEEE Transactions on Power Electronics*, vol. 28, no. 4, pp. 1900–1913, 2013.
17. Y. P. Hsieh, J. F. Chen, T. J. Liang, and L. S. Yang, “A novel high step-up dc–dc converter for a microgrid system,” *IEEE Transactions on Power Electronics*, vol. 26, pp. 1127–1136, April 2011.
18. C. D. Lute, M. G. Simoes, D. I. Brandao, A. Al Durra, and S. Muyeen, “Development of a four phase floating interleaved boost converter for photovoltaic systems,” in *Energy Conversion Congress and Exposition (ECCE), 2014 IEEE*, pp. 1895–1902, IEEE, 2014.
19. M. Kabalo, D. Paire, B. Blunier, D. Bouquain, M. G. Simões, and A. Miraoui, “Experimental evaluation of four-phase floating interleaved boost converter design and control for fuel cell applications,” *IET power electronics*, vol. 6, no. 2, pp. 215–226, 2013.
20. V. Utkin, “Sliding mode control of dc/dc converters,” *Journal of the Franklin Institute*, vol. 350, no. 8, pp. 2146–2165, 2013.
21. C. Bruni, G. Dipillo, and G. Koch, “Bilinear systems: An appealing class of “nearly linear” systems in theory and applications,” *IEEE Transactions on automatic control*, vol. 19, no. 4, pp. 334–348, 1974.
22. Y. M. Roshan and M. Moallem, “Control of non-minimum phase load current in a boost converter using output redefinition,” *IEEE Transactions on Power Electronics*, vol. 29, no. 9, pp. 5054–5062, 2014.
23. Y. Massaoudi, E. Dorsaf, J.-P. Gaubert, D. Mehdi, and T. Damak, “Experimental implementation of new sliding mode control law applied to a dc–dc boost converter,” *Asian Journal of Control*, vol. 18, no. 6, pp. 2221–2233, 2016.
24. H. Sira-Ramírez and R. Silva-Ortigoza, “Sliding mode- δ modulation control of the boost converter,” *Asian Journal of Control*, vol. 7, no. 4, pp. 349–355, 2005.
25. R. Ashok and Y. Shtessel, “Control of fuel cell-based electric power system using adaptive sliding mode control and observation techniques,” *Journal of the Franklin Institute*, vol. 352, no. 11, pp. 4911–4934, 2015.
26. G. Escobar, R. Ortega, H. S. Ramirez, J. P. Vilain, and I. Zein, “An experimental comparison of several nonlinear controllers for power converters,” *IEEE Control Systems*, vol. 19, pp. 66–82, Feb 1999.
27. Y. Huangfu, S. Zhuo, F. Chen, and S. Pang, “Evaluation and fault tolerant control of a floating

- interleaved boost converter for fuel cell systems," in *Industry Applications Society Annual Meeting, 2016 IEEE*, pp. 1–7, IEEE, 2016.
28. R.-J. Wai and L.-C. Shih, "Design of voltage tracking control for dc–dc boost converter via total sliding-mode technique," *IEEE Transactions on Industrial Electronics*, vol. 58, no. 6, pp. 2502–2511, 2011.
 29. M. Ahmeid, M. Armstrong, S. Gadoue, and M. Al-Greer, "Computationally efficient self-tuning controller for dc-dc switch mode power converters based on partial update kalman filter," *IEEE Transactions on Power Electronics*, 2017.
 30. X. Li, M. Chen, H. Shinohara, and T. Yoshihara, "Design of an auto-tunable pid controller for buck converters through a robust h synthesis approach," *IEICE Communications Express*, vol. 5, no. 1, pp. 7–12, 2016.
 31. S. El Beid and S. Doubabi, "Dsp-based implementation of fuzzy output tracking control for a boost converter," *IEEE Transactions on Industrial Electronics*, vol. 61, no. 1, pp. 196–209, 2014.
 32. M. K. Kazimierczuk and A. Massarini, "Feed-forward control of dc–dc pwm boost converter," *IEEE Transactions on Circuits and Systems I: Fundamental Theory and Applications*, vol. 44, no. 2, pp. 143–148, 1997.
 33. M. K. Kazimierczuk and L. Starman, "Dynamic performance of pwm dc–dc boost converter with input voltage feedforward control," *IEEE Transactions on Circuits and Systems I: Fundamental Theory and Applications*, vol. 46, no. 12, pp. 1473–1481, 1999.
 34. G. Mademlis, G. K. Steinke, and A. Rufer, "Feed-forward-based control in a dc–dc converter of asymmetric multistage-stacked boost architecture," *IEEE Transactions on Power Electronics*, vol. 32, no. 2, pp. 1507–1517, 2017.
 35. A. Kugi and K. Schlacher, "Nonlinear h infin; controller design for a dc-to-dc power converter," *IEEE Transactions on Control Systems Technology*, vol. 7, pp. 230–237, Mar 1999.
 36. W.-J. Liu, "Decentralized sliding mode control for multi-input complex interconnected systems subject to non-smooth nonlinearities," *Asian Journal of Control*, vol. 20, no. 3, pp. 1171–1181, 2018.
 37. C. Zaafouri, B. Torchani, A. Sellami, and G. Garcia, "Uncertain saturated discrete-time sliding mode control for a wind turbine using a two-mass model," *Asian Journal of Control*, vol. 20, no. 2, pp. 802–818, 2018.
 38. H. Chung, S. Y. R. Hui, and K. K. Tse, "Reduction of power converter emi emission using soft switching technique," *IEEE Transactions on Electromagnetic Compatibility*, vol. 40, pp. 282–287, Aug 1998.
 39. F. Pareschi, R. Rovatti, and G. Setti, "Emi reduction via spread spectrum in dc/dc converters: State of the art, optimization, and tradeoffs," *IEEE Access*, vol. 3, pp. 2857–2874, 2015.
 40. Y. M. Alsmadi, V. Utkin, M. A. Haj-ahmed, and L. Xu, "Sliding mode control of power converters: Dc/dc converters," *International Journal of Control*, pp. 1–22, 2017.
 41. P. R. Mohanty and A. K. Panda, "Fixed-frequency sliding-mode control scheme based on current control manifold for improved dynamic performance of boost pfc converter," *IEEE Journal of Emerging and Selected Topics in Power Electronics*, vol. 5, no. 1, pp. 576–586, 2017.
 42. A. Abrishamifar, A. Ahmad, and M. Mohammadian, "Fixed switching frequency sliding mode control for single-phase unipolar inverters," *IEEE Transactions on Power Electronics*, vol. 27, no. 5, pp. 2507–2514, 2012.
 43. S.-C. Tan, Y. Lai, C. K. Tse, and M. K. Cheung, "A fixed-frequency pulsewidth modulation based quasi-sliding-mode controller for buck converters," *IEEE Transactions on Power Electronics*, vol. 20, no. 6, pp. 1379–1392, 2005.
 44. Y. Cheng and Y. He, "Comments on design of voltage tracking control for dc–dc boost converter via total sliding-mode technique," *IEEE Transactions on Industrial Electronics*, vol. 63, no. 12, pp. 7776–7776, 2016.
 45. A. R. Yasin, M. Ashraf, and A. I. Bhatti, "Fixed frequency sliding mode control of power converters for improved dynamic response in dc micro-grids," *Energies*, vol. 11, no. 10, p. 2799, 2018.
 46. V. Utkin, J. Guldner, and J. Shi, *Sliding mode control in electro-mechanical systems*, vol. 34. CRC press, 2009.
 47. H. J. Sira-Ramirez and M. Ilic, "A geometric approach to the feedback control of switch mode dc-to-dc power supplies," *IEEE Transactions on circuits and systems*, vol. 35, no. 10, pp. 1291–1298, 1988.